Aperiodic and oscillatory systems underpinning human domain-general cognition

Runhao Lu, Nadene Dermody, John Duncan, Alexandra Woolgar

MRC Cognition and Brain Sciences Unit, University of Cambridge, Cambridge, UK

Runhao.Lu@mrc-cbu.cam.ac.uk

Abstract

Domain-general cognitive systems are essential for adaptive human behaviour, supporting various cognitive tasks through flexible neural mechanisms. From decades of fMRI studies, we know that a particular network of frontoparietal brain regions plays a role in supporting many different kinds of cognitive activity, with increased activity and information coding in response to increasing task demands. However, it is not clear whether there is a corresponding domain-general electrophysiological response to demand, such as a change in aperiodic or oscillatory power. Here we used irregular-resampling auto-spectral analysis (IRASA) to separate the aperiodic and oscillatory components of MEG/EEG signals, and analysed them with multivariate pattern analysis (MVPA) to investigate their roles in domain-general cognition. We found that both aperiodic (broadband power, slope, and intercept) and oscillatory (theta, alpha, and beta power) components coded both task demand and content across three cognitive tasks. Aperiodic broadband power in particular strongly coded task demand, in a manner that generalised across all subtasks, suggesting that modulation of aperiodic broadband power may reflect a domain-general response to multiple sorts of cognitive demand. Source estimation suggested that increasing cognitive demand decreased aperiodic activity across most of the brain, with the strongest modulations partially overlapping with the frontoparietal multiple-demand network. In contrast, oscillatory activity in the theta, alpha and beta bands showed more localised patterns of modulation, primarily in frontal (beta, theta) or occipital (alpha, theta) regions. The spatial pattern of demand-related modulation was significantly correlated across space in individuals, with positive correlations between theta and beta power, while both were negatively correlated with alpha power. These results provide novel insights into the electrophysiological underpinnings of human domain-general cognition, suggesting roles for both aperiodic and oscillatory systems, with changes in aperiodic broadband power being the clearest domain-general electrophysiological correlate of demanding cognitive activity.

Introduction

Human cognition is accomplished by the joint contributions of both domain-general and highly specialized neural systems [1-3]. A specific set of frontoparietal regions is known to support domain-general cognition as these areas are co-activated during a variety of cognitive tasks, including working memory, task switching, inhibitory control, and many more [4-7]. We refer to this widely distributed

domain-general system as the multiple-demand (MD) network, highlighting its activation in response to various task demands [1, 2, 8, 9]. However, it is not known whether corresponding domain-general electrophysiological responses, such as those measured by magnetoencephalography (MEG) or electroencephalography (EEG), support different types of cognitive activity. Identifying these processes is important, as electrophysiological responses are directly generated from neuronal activity. Understanding these responses can help bridge the gap between well-studied large-scale brain networks and electrophysiological activity, and help understand the functional organization of the brain.

Neural activity obtained from MEG/EEG is a mixed signal consisting of both aperiodic (also referred to as "1/f-like" or fractal) and oscillatory components [10-12]. Although early studies treated aperiodic components as noise, current theories suggest that aperiodic activity may reflect widespread brain network excitability and the balance of excitatory and inhibitory neural activity (E/I balance) [13, 14], and potentially underlie the network- and global-level signals observed in fMRI [15, 16]. Moreover, recent findings suggest that aperiodic activity plays functional roles in various cognitive processes like perception, attention, working memory, memory consolidation, cognitive processing speed, and cognitive demand [10, 11, 14, 17-22]. Notably, a recent study found that aperiodic activity outperformed oscillatory power and cross-frequency phase-amplitude coupling in indexing cognitive load variation during a counting task, with lower aperiodic slope and intercept associated with higher load [22]. These findings highlight the potential significance of aperiodic activity in fundamental cognitive processes. However, it remains largely unknown whether aperiodic activity responds to task demand across multiple tasks (thus supporting domain-general cognition) and where demand-related aperiodic signals are located in the brain.

For oscillatory activity, many MEG/EEG studies have found that neural oscillations at different frequency bands are associated with task demand in various tasks [23-26]. Interestingly, a body of findings suggests that oscillatory power in many different frequency bands, such as theta (3-7 Hz), alpha (8-12 Hz), and beta (15-30 Hz), is modulated by task demand, with either increased or decreased power (e.g., theta [27-32]; alpha [33-38]; beta [39-42]). However, it is not yet clear to what extent these demand-related responses are similar between tasks, reflecting a domain-general property for cognitive control. Additionally, as most of the previous studies have not separated aperiodic and oscillatory activity, it is uncertain to what extent the reported results specifically reflect modulations of oscillatory activity in bands, or changes in global aperiodic activity, or both [10, 12].

In addition to being more active during difficult compared to easy cognitive tasks, the domain-general MD network is also known to encode various types of task-relevant information beyond demand, such as details of task stimuli, task rules, and response information [1, 43-46]. Indeed, non-human primate studies indicated that MD neurons exhibit mixed selectivity, in which their responses reflect non-linear combinations of different task elements, adaptively coding multiple task features with high dimensionality [47-49]. Therefore, if we identify any candidate domain-general aperiodic or oscillatory activity reflecting task-demand across multiple tasks, it would be interesting to know whether these electrophysiological responses also code other information such as the stimuli used in each task. If so, this would make the responses domain-general in terms of informational content as well as domain-general in terms of reflecting demand across multiple cognitive tasks.

To address these questions, we recorded neural signals using combined MEG/EEG while participants performed three cognitive tasks, each with two different sets of stimuli and two levels of demand. Using irregular resampling auto-spectral analysis [50] (IRASA), we extracted aperiodic components indexed by three parameters (broadband power, slope, and intercept) and oscillatory power in three canonical frequency bands (theta, alpha, and beta). We then asked whether any aperiodic or oscillatory components coded task demand (hard vs. easy) across all the subtasks using multivariate pattern analysis (MVPA) [51, 52]. Next, we investigated whether these responses in one subtask could be generalised to other subtasks, indicating a domain-general property. To explore the spatial distribution of these signals, we estimated their demand-related cortical source patterns and compared these patterns across different subtasks and oscillatory bands. Finally, we examined whether these demand-related electrophysiological signals simultaneously code task content information (alphanumeric vs. colour) with similar source patterns, demonstrating the adaptive coding property akin to that of the domain-general MD network [1, 43, 45, 46].

Results

Behavioural results

Our primary goal was to investigate potential aperiodic and oscillatory signals reflecting change in task demand across multiple cognitive tasks. We therefore employed three cognitive tasks (Figure 1A), which were a working memory task (WM), a switching task (SWIT) and a multi-source interference task (MSIT). Each task had two different stimulus contents (alphanumeric or colour

stimuli) and two levels of demand (hard vs. easy). This design resulted in six subtasks (3 tasks * 2 contents).

To verify the demand manipulation, we conducted 2 (task demand: hard vs. easy) * 2 (task content: alphanumeric vs. colour) repeated measures ANOVAs on behavioural accuracy and reaction time (RT) for each task. Indeed, there was a significant main effect of task demand on accuracy for all three tasks, showing that participants were more accurate in easy conditions than in hard conditions [Figure 1B WM: F (1,42) = 106.63, $p < 0.001$, $\eta_p^2 = 0.72$; SWIT: F (1,42) = 11.49, $p = 0.002$, $\eta_p^2 = 0.22$; MSIT: F (1,42) = 54.66, $p < 0.001$, $\eta_p^2 = 0.57$; see Table S1 for descriptive statistics]. Similarly, there was a significant main effect of task demand on RT for all three tasks, showing that participants had slower RT in hard conditions compared to easy conditions [WM: F (1,42) = 207.15, $p < 0.001$, $\eta_p^2 = 0.83$; SWIT: F (1,42) = 114.11, $p < 0.001$, $\eta_p^2 = 0.73$; MSIT: F (1,42) = 437.87, $p < 0.001$, $\eta_p^2 = 0.91$; see Table S1 for descriptive statistics]. These results confirmed the validity of task demand manipulation across all tasks.

We then examined whether participant's accuracy and RT varied with task content. For behavioural accuracy we did not find a significant content effect or interaction between task demand and content on accuracy in the SWIT [content effect: F (1,42) = 0.01, $p = 0.94$; interaction: F (1,42) = 0.02, $p = 0.90$] or MIST tasks [content effect: F (1,42) = 1.11, $p = 0.30$; interaction: F (1,42) = 3.67, $p = 0.06$]. However in the WM task, we found a significant main effect of task content [F (1,42) = 21.80, $p < 0.001$, $\eta_p^2 = 0.34$] and a significant interaction between task demand and task content [F (1,42) = 31.69, $p < 0.001$, $\eta_p^2 = 0.43$]. Participants were significantly less accurate in the colour WM task than that in the alphanumeric WM task in the hard condition [F (1,42) = 32.49, $p < 0.001$] but not in the easy condition [F (1,42) = 0.20, $p = 0.65$]. For RT, we found a significant content effect in the WM tasks [F (1,42) = 50.16, $p < 0.001$, $\eta_p^2 = 0.54$] and the MSIT tasks [F (1,42) = 5.83, $p = 0.02$, $\eta_p^2 = 0.12$]. Participants had slower RT in the colour compared to alphanumeric MSIT tasks, and they had faster RT in the colour compared to alphanumeric WM task. The WM result may have reflected a speed-accuracy trade-off in the WM tasks, in that participants tended to respond faster in the colour task but with lower accuracy (at least in the hard condition). We did not find a significant content effect on RT in the SWIT tasks [F (1,42) = 0.46, $p = 0.50$] or interactions between demand and content in any tasks [all Fs < 1.84, ps > 0.18].

The behavioural results therefore indicated that hard conditions were more demanding than easy

ones across all tasks, as intended. Task performance was similar for the alphanumeric and colour versions of each task, with the exception of the WM task in which there appeared to be a speed-accuracy trade-off in which participants were slightly faster and substantially less accurate in the colour version of the high demand task. Participants also tended to respond more quickly in the alphanumeric MSIT task compared to the colour MSIT task.

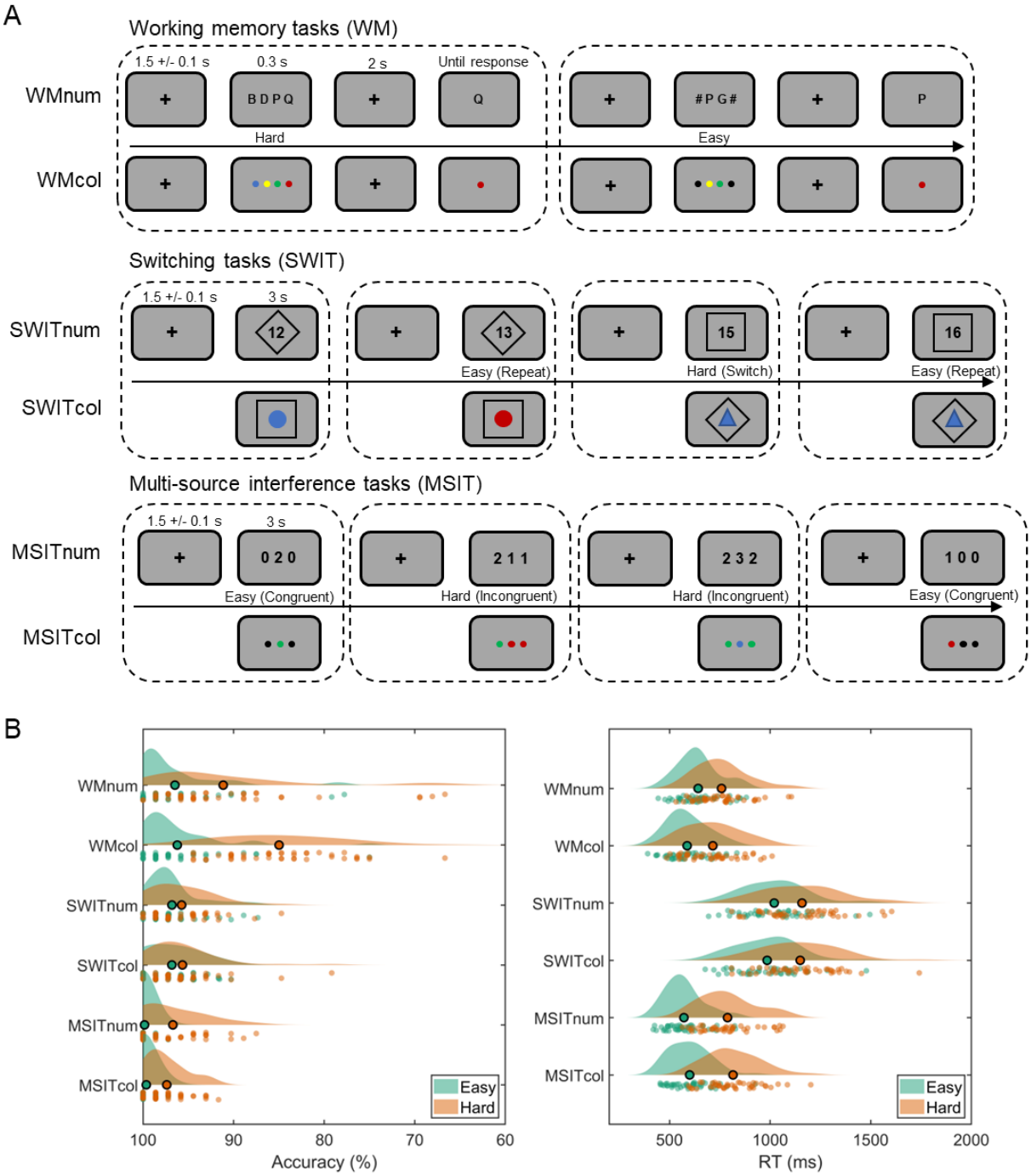

Figure 1. Experimental paradigm and behavioural results.
(A) Experimental design of the working memory task (WM), the switching task (SWIT), and the multi-source interference task (MSIT). Each task had two versions with either alphanumeric or colour stimuli as task contents.

For the WM task, participants were required to remember either four items (hard condition) or two items (easy condition). The items were letters in the alphanumeric condition and were coloured circles in the colour condition. For the SWIT task, participants made responses based on the current rule indicated by the shape (a square or a diamond) that surrounded the item. Switch trials (the rule for the present trial differed from the last trial) were considered the hard condition, and repeat trials (the rule for the present trial repeated the last trial) were considered the easy condition. For the MSIT task, participants needed to identify the unique item among three presented items. In the easy (congruent) condition, the target item was presented in the position compatible with its original value (e.g., "100" or "red, black, black"). In the incongruent (hard) condition, the target item was presented in the position incongruent with the original value and always flanked by different interfering numbers or colours (e.g., "331" or "blue, blue, red"). (B) Behavioural accuracy (left) and response time (RT; right) in easy and hard conditions for each subtask. Each individual dot in the raincloud plots represents a participant and the bolded dot shows the mean. Repeated measures ANOVAs (task demand * task contents) showed that the main effects of task demand (hard vs. easy) were significant for both accuracy and RT for all 6 subtasks (all ps < 0.002).

Domain-general coding of task demand by aperiodic components

To obtain the aperiodic and oscillatory neural components in MEG/EEG data, we first subtracted evoked potentials of each condition from the MEG/EEG signal to remove evoked and phase-locked activity [29]. Then, we applied the IRASA [50] on the time windows of 0.3-1.5 second from stimulus onset for each task to separate the aperiodic and oscillatory components from the mixed signal (Figure 2A).

First, we used MVPA to ask whether we could decode task demand based on three parameters that describe the aperiodic component of the signal (3-30 Hz broadband power, slope, and intercept) across MEG/EEG sensors. Indeed, as shown in Figure 2B, we could decode task demand from all three aperiodic parameters across all subtasks with significant above-chance areas under the receiver operating characteristic curve (AUC) (all ts > 5.19; FDR-corrected ps < 0.001). For all signals, the AUC was relatively high in the WM and MSIT tasks but lower in the SWIT tasks. Aperiodic broadband power, which reflects both the slope and intercept, tended to show the highest AUC.

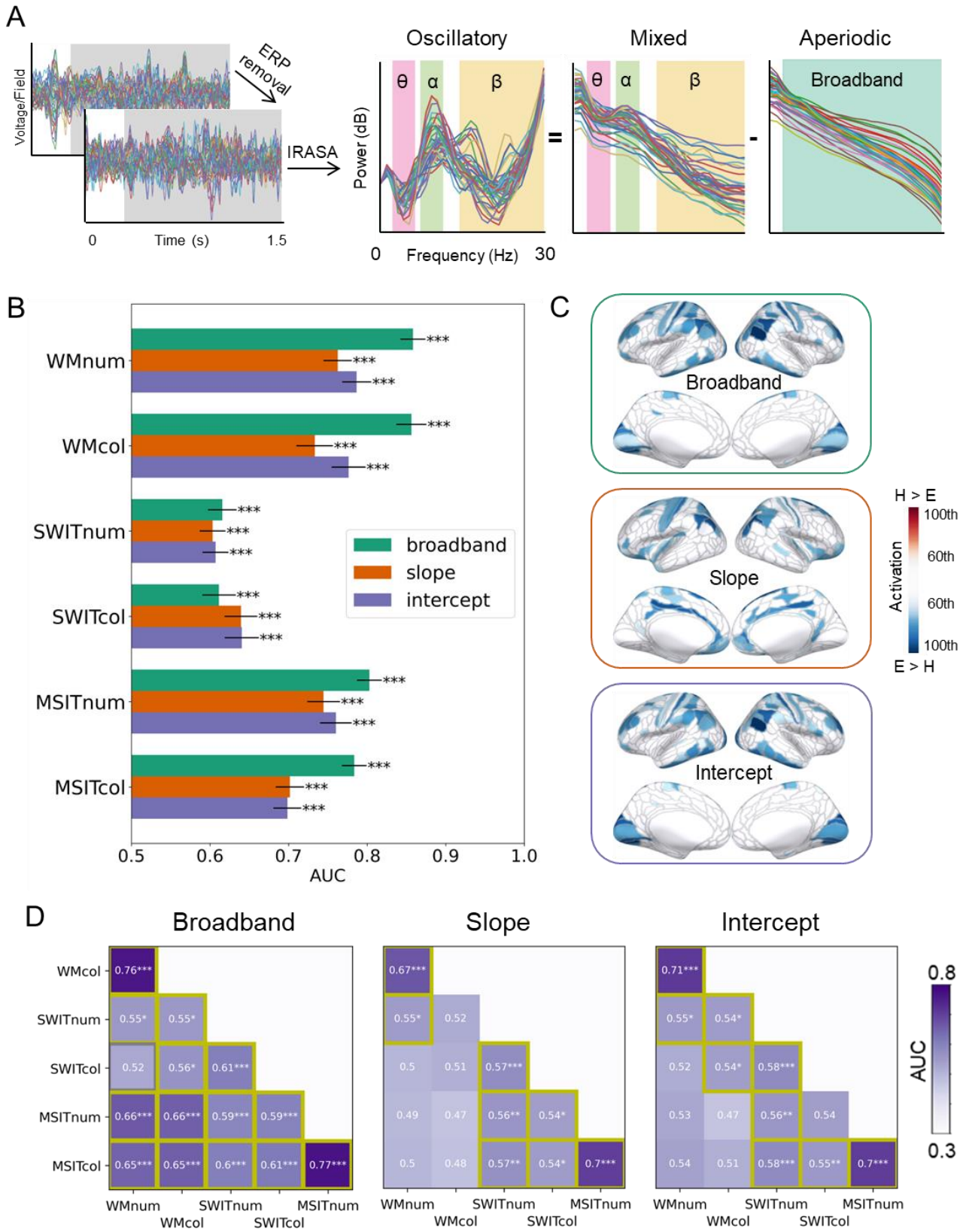

Figure 2. Domain-general coding of task demand by aperiodic components.

(A) To separate the aperiodic and the oscillatory components from the mixed signal, we first subtracted the event-related potentials from the timeseries data for each condition to remove the phase-locked evoked signals. Then, we used irregular resampling auto-spectral analysis (IRASA) based on the time window of 0.3-1.5 second

from stimulus onset to obtain the aperiodic components in the frequency domain. After subtracting the aperiodic components from the mixed activity, we obtained the oscillatory components in the frequency domain. We selected theta (3-7 Hz), alpha (8-12 Hz), and beta (15-30 Hz) as the frequencies of interest for further analyses. For the aperiodic components, we used the broadband power (3-30 Hz), slope, and intercept for further analyses (both slope and intercept were obtained from the linear function that best fitted the aperiodic power spectrum) (B) Decoding results on task demand (hard vs. easy) using aperiodic activity for each subtask. All MEG/EEG sensors were used for decoding. Error bars represent standard errors. (C) Source estimation patterns for demand decoding averaged across all the subtasks for aperiodic signals. Outlines show 360 cortical regions based on the Human Connectome Project multimodal parcellation (HCP-MMP1.0) [53]. Coloured regions represent the 60th to 100th percentiles of activation (hard vs. easy discrimination) across the brain (H: hard; E: easy). Negative (blue) values indicate decreased activity (or a steeper slope) in the hard condition compared to the easy condition. The full map and source estimation patterns for each subtask separately are shown in Figure S1. (D) Cross-task generalisation of task demand coding based on aperiodic activity. All MEG/EEG sensors were used for decoding. Classifiers were trained in one subtask and then tested in other subtasks with the same signal. Each coloured box represents the average of the generalisation performance between two paired train-test schemes within a pair of subtasks (e.g., training on A, testing on B and training on B, testing on A), with significantly above-chance AUC (highlighted with yellow borders) meaning the signal was generalisable across the two tasks. WM: Working memory task; SWIT: Switching task; MSIT: Multi-source interference task; num: Alphanumeric task; col: Colour task. * $p < 0.05$, ** $p < 0.01$, *** $p < 0.001$ (FDR-corrected).

Next, we quantified the extent to which the effect of demand was comparable across subtasks. To address this, we performed a cross-task generalisation of demand classification in sensor space, where we by turns trained classifiers to distinguish task demand on one subtask and tested them on other subtasks (see Methods). If task demand has a similar effect on activity across subtasks, we should see above-chance AUC for cross-task generalisations. As shown in Figure 2D, we found consistent above-chance generalisability for broadband power across all different subtasks except between the colour SWIT and alphanumeric WM tasks. Thus, with one exception, the effect of demand on broadband aperiodic power was demonstrably similar across the three different cognitive tasks and their stimulus variations. The slope and intercept parameters of the aperiodic components showed generalisability between different contents of the same task (e.g., WM tasks with alphanumeric or colour contents), and between SWIT and MSIT across tasks and contents.

We then estimated the cortical sources of these demand-coding aperiodic signals. For this, we estimated the source space responses for each individual, parcellated into 360 regions of interest (ROIs; 180 regions per hemisphere without the medial wall) based on the Human Connectome Project multimodal parcellation (HCP-MMP1.0) [53]. We then re-ran the demand decoding analysis using the activity in all these source-level ROIs and transformed the resulting classifier weights, by multiplying

them with the covariance of the data, to yield interpretable values reflecting the signal contributed by each source ROI to the classification [54] (see Methods). Positive values indicated increased activity in the hard condition compared with the easy condition. To illustrate the sources contributing to the decoding of task demand, we averaged the patterns across all the six subtasks for each signal and visualised the most informative regions, corresponding to the 60th to 100th percentiles, on an inflated template brain (Figure 2C, see also Figure S1A for the full unthresholded map).

The most informative regions underpinning demand coding in aperiodic broadband power and intercept were similar to one another (Figure 2C, top and bottom panel). They showed a widely distributed spatial pattern with decreases in lateral frontoparietal MD-like regions, motor regions, and visual regions. The most informative regions for aperiodic slope were somewhat different from the other two aperiodic parameters, mainly located in the cingulate cortex, motor regions, and parietal regions. This spatial pattern of demand-related aperiodic activity was highly consistent across the six subtasks (Figure S1B), suggesting a domain-general aperiodic responses to increased cognitive demand.

In summary, we found that aperiodic activity coded task demand across all subtasks with decreased aperiodic responses to increasing cognitive demand across widespread sources irrespective of the particular cognitive task or stimulus content. Moreover, a classifier showed strong cross-task generalisation of aperiodic activity, especially as captured by broadband power, in the pattern of change over subtasks. These results suggest that aperiodic activity could play a domain-general role in supporting cognition.

Coding of task demand by oscillatory power

We then asked how demand modulated oscillatory responses. For this we used MVPA to quantify whether oscillatory power in different frequency bands (theta: 3-7 Hz; alpha: 8-12 Hz; beta: 15-30 Hz) was modulated by task demand. As above, we used data calculated from all the MEG/EEG sensors and performed the demand decoding analysis on each subtask separately. As shown in Figure 3A, we found that oscillatory power in all three frequency bands could code task demand across all subtasks with significantly above-chance AUC (all ts > 3.22; FDR-corrected ps < 0.002). AUC was again relatively high in the WM and MSIT tasks compared to the SWIT task. Interestingly, oscillatory components tended to show lower AUC than aperiodic components in general.

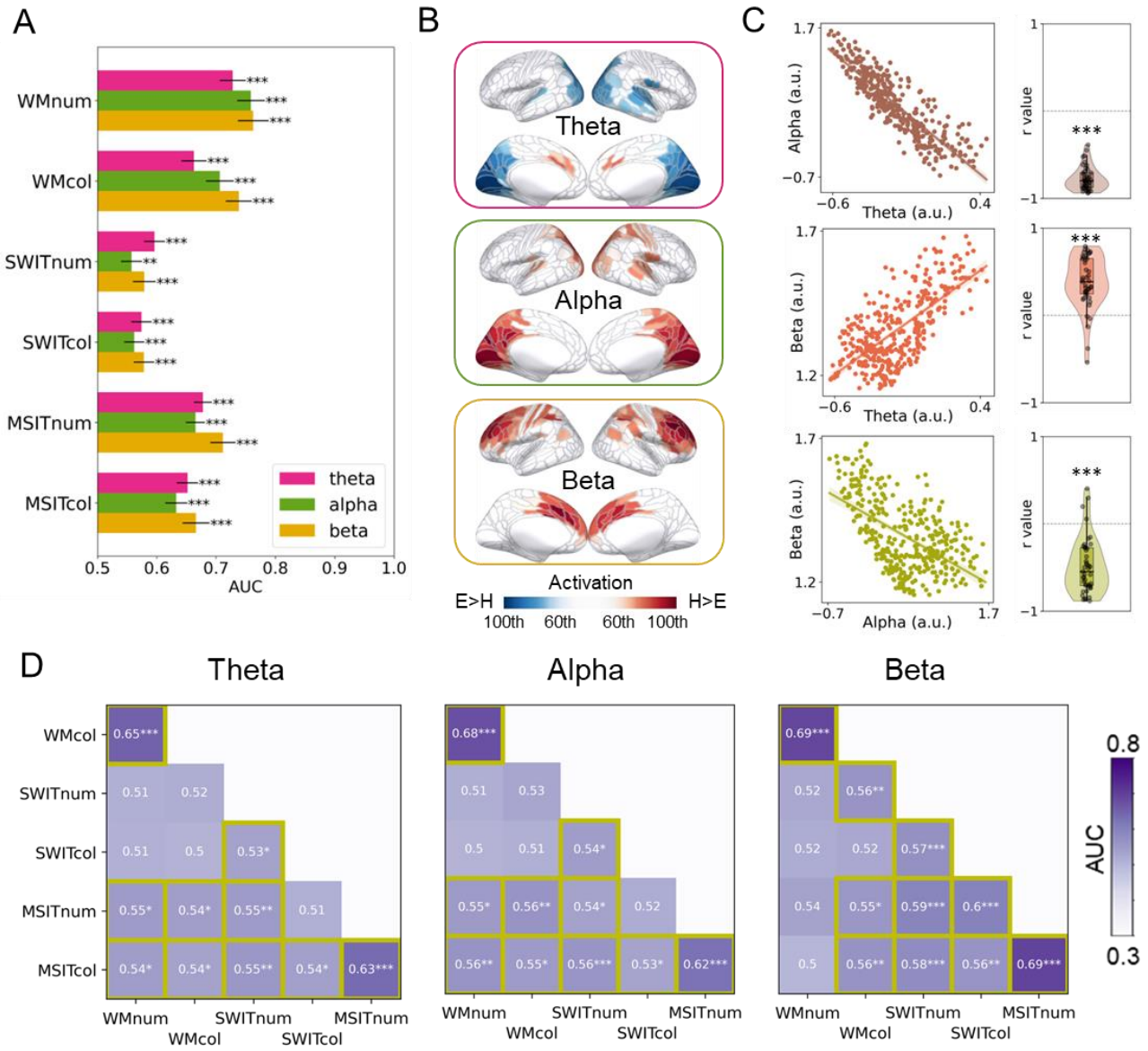

Figure 3. Coding of task demand by oscillatory power

(A) Decoding of task demand (hard vs. easy) using oscillatory activity for each subtask. All MEG/EEG sensors were used for decoding. Error bars represent standard errors. *** $p < 0.001$ (FDR-corrected). (B) Source estimation patterns for demand decoding averaged across the subtasks for the oscillatory signals. Coloured regions represent the 60th to 100th percentiles of activation (hard vs. easy discrimination) across the brain (H: hard; E: easy). Positive (red) values indicate increased activity (or a shallower slope) in the hard condition compared to the easy condition. Source estimation patterns for the full map (0th to 100th percentiles) and for each subtask separately are shown in Figure S2. (C) Pearson's correlation between source estimation patterns (360 ROIs in source space) that coded task demand from oscillatory power in different frequency bands. Left: Scatter plots using data averaged across subtasks and participants for illustration. Each dot represents a cortical ROI. Right: Correlation coefficients from within-subject analyses, each dot represents a single participant. *** $p < 0.001$ with 1000 permutations (D) Cross-task generalisation of task demand using oscillatory activity from all MEG/EEG sensors. Classifiers were trained on one subtask and then tested on other subtasks with the same signal. The results show the generalisation between different tasks, with significantly above-chance AUC (highlighted with yellow borders) meaning the signal was generalisable across the two tasks. Abbreviations as

in Figure 2. * $p < 0.05$, ** $p < 0.01$, *** $p < 0.001$ (FDR-corrected).

Cross-task generalisation results indicated that the three bands of oscillatory power exhibited generalisability across some but not all subtasks (Figure 3D). In particular, they all showed high generalisability between different contents of the same task. Additionally, oscillatory power in all three frequency bands generally showed generalisability between MSIT and SWIT tasks, with a couple of exceptions, but tended to show a lack of generalisation between WM and SWIT, and for beta between the alphanumeric WM task and any version of SWIT or MSIT. These findings suggested that the oscillatory components might code task demand through a combination of shared and distinct patterns across tasks. These codes are generalisable for some tasks but may change in other specific tasks.

We then estimated the source patterns of demand-related oscillatory power in each frequency band (Figure 3B and Figure S2A). We found increased demand-related theta power in the medial frontal regions under hard conditions, along with a decrease in theta power in occipital regions. Alpha power, instead, showed an increase in the occipital regions. Beta power mainly showed an increase in the lateral and medial frontal regions.

To quantitatively examine the inter-correlations among the three oscillatory components, we correlated the subtask-averaged source patterns over the 360 parcels in each individual separately, and then compared the distribution of resulting Pearson's r values to chance using permutation tests. (Figure 3C). The distribution of activation patterns over spatial sources was significantly anticorrelated between theta and alpha (mean r = -0.77 across participants, $p < 0.001$ with 1000 permutations), correlated between theta and beta (mean r = 0.38 across participants, $p < 0.001$ with 1000 permutations), and anticorrelated between alpha and beta (mean r = -0.48 across participants, $p < 0.001$ with 1000 permutations).

When separately examining the source patterns for each subtask (Figure S2B), we found that demand-related oscillatory power showed broadly consistent spatial patterns across subtasks, with minor specific patterns differentiating the subtasks. For example, theta power had a stronger demand-related increase in medial frontal regions during the SWIT and MSIT but not WM tasks, while alpha power showed a demand-related increase in motor regions that was more pronounced in the two WM subtasks than the other tasks.

To summarize, these results indicated that oscillatory power in theta, alpha, and beta bands were also modulated by task demand with fairly consistent source patterns across subtasks but with some

task-based idiosyncrasies. Although oscillatory power showed good cross-generalisability for some tasks, decoding tended to be weaker than we had seen for aperiodic activity (especially broadband aperiodic power) and could not generalise across all the tasks, suggesting that there might be both shared and task-specific responses to different types of cognitive demand.

Coding of task content by aperiodic and oscillatory components

In addition to responding to a range of different task demands, a domain-general system may be expected to code task-relevant information across multiple tasks [44, 55]. Therefore as a final set of analyses, we examined whether aperiodic and oscillatory components of the MEG/EEG signals also coded task content information (alphanumeric vs. colour).

As shown in Figure 4A and 4B, we found that, in sensor space, both aperiodic and oscillatory components showed significant above-chance AUC for decoding task content across the three tasks (aperiodic: ts > 15.31; FDR-corrected ps < 0.001; oscillatory: ts > 4.77; FDR-corrected ps < 0.001), indicating that all these signals also reflected task content. The decoding profiles were similar across different tasks for both aperiodic and oscillatory results. For aperiodic components, broadband power again showed the highest AUC, while intercept showed the lowest but still above-chance AUC. For oscillatory power, numerically beta band showed the highest AUC, while theta band showed the lowest but still above-chance AUC. In general, the aperiodic components again tended to show higher AUC than the oscillatory components.

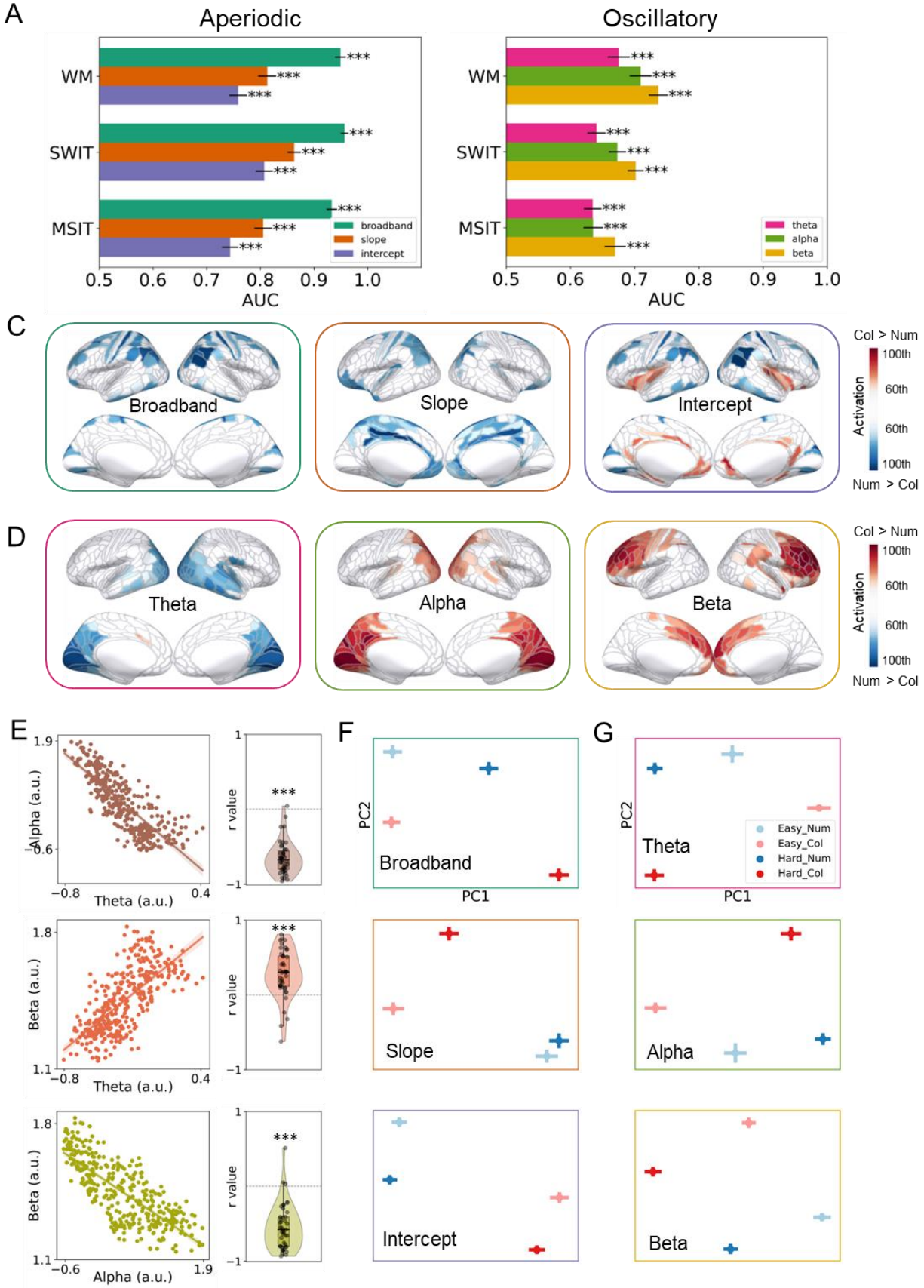

Figure 4. Aperiodic and oscillatory components code task content

(A, B) Decoding of task content (alphanumeric vs. colour) using (A) the aperiodic and (B) the oscillatory activity

for each task. All MEG/EEG sensors were used for decoding. Error bars represent standard errors. *** $p < 0.001$ (FDR-corrected). (C, D) Source estimation patterns for content decoding averaged across all tasks for (C) aperiodic and (D) oscillatory signals. Coloured regions represent the 60th to 100th percentiles of activation (colour vs. alphanumeric discrimination) across the brain. Positive values (red) indicate increased activity (or a shallower slope) in the colour condition compared to the alphanumeric condition. Source estimation patterns for each task separately are shown in Figure S4. (E) Pearson's correlation results between source estimation patterns (360 ROIs in source space) that coded task content from oscillatory power in different frequency bands. Left: Scatter plots using data averaged across subtasks and participants for illustration. Each dot represents a cortical ROI. Right: Correlation coefficients from within-subject analyses, each dot represents a single participant. *** $p < 0.001$ with 1000 permutations. (F, G) Representations of task demand and task content in two-dimensional space extracted from (F) the aperiodic and the (G) oscillatory signals from all MEG/EEG sensors. Abbreviations as shown in Figure 2.

Next we examined the source distribution of the patterns. As shown in Figure 4C and 4D, we found that the cortical patterns that contributed to task content classification were visually similar to those found in decoding task demand (Figure 2C and Figure 3B). To quantify this, we calculated Pearson's correlations across the 360 ROIs between task-averaged demand and content decoding patterns for both aperiodic and oscillatory signals for each individual, and then compared the resulting distribution of r values to chance using 1000 permutations (Figure S3; see Methods). Results showed that demand and content decoding patterns in source space were significantly correlated for both aperiodic (mean $r = 0.82$, 0.66, and 0.83 across participants, respectively, for broadband power, slope, and intercept; all ps < 0.001 with 1000 permutations) and oscillatory signals (mean $r = 0.81$, 0.81, and 0.72 across participants, respectively, for theta, alpha, and beta; all ps < 0.001 with 1000 permutations). Specifically, the source patterns of aperiodic broadband power and intercept for classifying task content again showed a wide range of cortical contribution across the frontoparietal MD-like regions and the cingulo-opcular regions. The aperiodic slope mainly showed spatial patterns in frontal, cingulate, and parietal regions. For oscillatory power, theta power that responded to task content mainly originated from visual regions; alpha power showed a reversed patterns to theta but also located in the occipital regions; and beta power mainly came from the lateral and medial prefrontal regions. We also separately examined the source patterns for each task (Figure S4), and they showed similar patterns to the averaged pattern across tasks.

To further understand the inter-correlations among oscillatory power based on their source patterns across 360 cortical regions, we again performed Pearson's correlations (Figure 4E). As for demand, the distribution of activation patterns over spatial sources that supported content coding was significantly anticorrelated between theta and alpha, correlated between theta and beta, and

anticorrelated between alpha and beta (mean r = -0.65, -0.28, and -0.54 across participants, respectively; all ps < 0.001 with 1000 permutations).

It should be noted that the behavioural accuracies of the alphanumeric tasks and the colour tasks were not strictly matched, especially for the hard condition in the WM tasks. To exclude the potential confounds of task demand in classifying contents, we repeated the analysis using only easy trials to decode task content, as the behavioural accuracies in the easy conditions were well matched across subtasks. The decoding results based on easy trials only, as well as their source estimations, showed very similar patterns to the results above (Figure S5).

Since both task demand and content were simultaneously coded by aperiodic and oscillatory components, we further visualised their representational geometry in two-dimensional space based on all MEG/EEG sensors. We averaged trials within each condition (12 conditions in total: 3 tasks * 2 demands * 2 contents) for each sensor and each signal, then performed principal component analysis (PCA) to extract the first two principal components (PCs) for visualization (see Methods). Figure 4F and 4G show the representations of task demand and task content (averaged across three tasks) in each signal. For both aperiodic and oscillatory signals, there was a clear boundary between the alphanumeric tasks (shown in blue) and the colour tasks (shown in red). Also, there was clear separation of easy (shown in light colours) and hard (shown in dark colours) trials for each subtask. These results indicate that although both task demand and content could be decoded from aperiodic and oscillatory signals, their coding dimensions appeared to be distinct.

Taken together, these results indicate that both aperiodic and oscillatory components reflect task demand and task content across multiple tasks. Source estimation results showed that the cortical patterns in support of task content classification were generally similar to those supporting task demand classification. Moreover, representational geometry results suggested that aperiodic and oscillatory systems code demand and content with different coding dimensions. These results together indicate that the same domain-general aperiodic and oscillatory systems can simultaneously code various task-relevant information, likely using different coding dimensions to support cognition.

Discussion

Using MEG/EEG recording in combination with IRASA and MVPA, the present study asked whether the human brain exhibits domain-general aperiodic and/or oscillatory responses to multiple

types of cognitive challenge. We recorded MEG/EEG signals when participants performed three different cognitive tasks (the WM, SWIT, and MSIT tasks) each with different levels of demand (hard vs. easy) and content (alphanumeric vs. colour). Decoding results showed that both aperiodic (broadband power, slope, and intercept) and oscillatory (in theta, alpha, and beta) components were modulated by task demand and content across all subtasks, with the patterns of demand modulation generalizable among the different tasks. Aperiodic broadband power showing the strongest cross-subtask generalisability, suggesting that it may reflect a domain-general mechanism supporting cognitive control. These results echo previous studies that showed modulation of aperiodic and oscillatory activity with task demand [22-25], and particularly emphasise the relevance of aperiodic components of electrophysiological activity.

The aperiodic 1/f-like spectral pattern has been observed ubiquitously in nature and across many different modalities of neural activity [11, 20, 56]. Although aperiodic activity was previously considered to reflect noise, an increasing number of studies have found roles for aperiodic activity in a wide range of cognitive processes including perception, attention, working memory, cognitive load, aging-related cognitive changes, and more [11, 14, 17-22, 57-60]. One recent study compared the role of aperiodic activity and alpha oscillations in predicting processing speed, and found it was the aperiodic rather than oscillatory alpha activity that predicted processing speed [19]. Another study associated different EEG indices with cognitive load in a counting task, finding that aperiodic activity outperformed both oscillatory power and cross-frequency phase-amplitude coupling [22]. Our results are consistent with these findings and further suggest that aperiodic activity coded both demand and content in a way that generalised across multiple tasks, suggesting a domain-general property.

To examine the potential cortical distribution of the demand- and content-related aperiodic activity, we performed source estimation and found a wide-distributed pattern of aperiodic activity across many brain regions. Interestingly, the patterns of aperiodic broadband power and intercept partly overlapped with the frontoparietal MD regions, potentially linking the domain-general MD network with domain-general electrophysiological signals. The frontoparietal distribution of aperiodic signals align with previous research [61]. Notably, although BOLD signals in the MD network increase with task demand [2, 8], we found that aperiodic activity in the MD network appeared to decrease with task demand. This result is in line with previous findings in both EEG and fMRI that both aperiodic slope and intercept were decreased in high cognitive load conditions [11, 61-63], supporting the hypothesis

that stronger aperiodic (or 'fractal') properties may reflect more rested and less effort state [61, 63]. Consistent with this, a recent study using simultaneous resting-state EEG-fMRI found that aperiodic EEG components were negatively correlated with BOLD activation in frontal and parietal regions while positively correlated in the insula and cingulate regions [16]. This implies that aperiodic activity might be related to BOLD activation observed in fMRI, though not necessarily in the same direction. The canonical finding of increased BOLD activation in the MD network [2, 8] might be expected to reflect demand related decreases consistent with the pattern we observed here. Future studies could use multimodal methods (e.g., concurrent EEG-fMRI and MEG/EEG-fMRI fusion) to further probe the relationships between task-based fMRI BOLD signals and the broadband aperiodic components of MEG/EEG signals. Meanwhile, as we found aperiodic broadband power showed a wide-spread decrease in hard conditions, there is another possibility that this may reflect a general reduction in noise when people need to focus. However, we think it is not very likely as noise is typically random and unstructured. Instead, our results not only showed that aperiodic broadband power codes both demand and content, but also demonstrated that it codes demand and content in a fairly structured way (i.e., orthogonal separations for content and demand coding; as shown in Figure 4F and 4G). This indicates that aperiodic activity is a meaningful signal in coding task demand and content rather than pure noise.

MEG/EEG oscillatory power has also been linked to various cognitive processes [23, 41, 64, 65]. Although many studies have attempted to associate oscillatory power in different frequency bands with task demand, there remains ongoing debate about how oscillations in different bands are modulated by demands of various tasks, particularly regarding their cortical distributions and modulation directions [23-25]. One key factor contributing to this discrepancy is the potential confound of the aperiodic component [10, 12, 66]. In this study, we separated oscillatory activity from the aperiodic background and systematically examined the role of pure oscillatory power in coding demand across multiple tasks. We found that with increasing task demand, theta power increased in the medial frontal regions and anterior cingulate cortex (ACC). This aligns with the classic theory about mid-frontal theta in cognitive control [23] and empirical studies showing that mid-frontal theta increases with higher task engagement [28, 30, 67-69]. Additionally, we observed a decrease in theta power in the occipital regions with higher demand, which potentially reflects information exchange between frontal and occipital regions [70, 71].

Compared with theta, how alpha and beta power are modulated by task demand remains debated, with studies often showing contradictory evidence regarding the direction of change [24, 25]. By examining the decoding from pure oscillatory power, we found alpha power increased with task demand in the occipital regions, consistent with previous findings on the load effect on occipital alpha increase [72, 73]. A simultaneous EEG-fMRI study similarly showed that alpha power that increased with cognitive load originated in the early visual areas [74]. The increased alpha oscillations in visual areas might reflect the functional inhibition of early visual areas that are not currently required for the task [75]. For beta power, we found an increase in frontal regions with increasing task demand, consistent with a series of previous findings [40-42]. Intracranial studies have linked beta oscillations in local field potentials to top-down cognitive control supporting behaviour [39, 76, 77]. An increase in frontal beta oscillations may thus reflect enhanced recruitment of top-down control. Together, our findings provide new insights into the debate on the relationship between oscillatory power and task demand by isolating pure oscillatory power from the aperiodic background. Moreover, by examining multiple tasks, we provide evidence that theta, alpha, and beta power can code both demand and content across many tasks. However, their coding strength and cross-task generalisability tended to be weaker compared to aperiodic activity.

Interestingly, we found that the source distributions for both aperiodic and oscillatory components in content coding were similar to the patterns for demand coding. This finding highlights their domain-general properties, indicating that these components can simultaneously code multiple aspects of task-relevant information. This is consistent with the observations in previous fMRI and non-human primate results, which showed that the domain-general MD network could flexibly code diverse information including visual, auditory, rule, and response [1, 44-46]. When examining their representation geometry in coding both demand and content, we found two clear and distinct classification boundaries for decoding demand and content. This result first confirmed that the above-chance content decoding was not merely a consequence of different demands in the tasks, and further suggested that these signals may code different task-relevant information using distinct coding dimensions to avoid inference [78, 79].

As oscillatory power in different frequency bands all contributed to demand and content decoding, we also examined their inter-relationships. For both demand and content decoding, we found that the spatial distribution of theta power showed a positive correlation with beta power, while both theta and

beta patterns showed negative correlations with alpha. In particular, with increased task demand, theta showed increase in medial frontal regions and decrease in occipital regions, while alpha showed a reversed pattern. Beta generally showed increase across the brain with increased demand, with the strongest increase in frontal regions. Previous studies have reported contradictory results regarding the relationship between theta and alpha, with many studies showing reversed patterns between them as we did [80, 81], but some studies showed comparable patterns between them [72, 82]. A recent study found that the cortical patterns of theta and alpha power in coding perception-action representations were generalisable across these two frequency bands, indicating their potential functional similarities [82]. However, as mentioned above, most of these studies did not separate oscillatory and aperiodic components before examining the relationship between different frequency bands, which makes the results challenging to interpret. Due to the homogeneity of the broadband aperiodic power, oscillations in different frequency bands may tend towards showing positive correlations if the aperiodic components are not separated out. After separating aperiodic components from the oscillatory activity, our results provided more compelling evidence that the spatial distributions of theta and beta power are positively correlated, while both are negatively correlated with alpha power.

In conclusion, this study suggests that both aperiodic and oscillatory components of human electrophysiological signals may reflect domain-general responses to demand and change in task content. Notably, aperiodic broadband power showed the strongest domain-general properties with robust coding of both demand and content and cross-task generalisability of these signals. The aperiodic and oscillatory systems had distinct source distributions, with the aperiodic broadband power being widely distributed across the brain and partially overlapping with the domain-general MD network, while oscillatory power was mainly modulated in frontal or occipital areas. Theta and beta power shared similar cortical patterns, whereas alpha power exhibited reversed patterns relative to the other two. These findings provide novel insights into the neural responses for human domain-general cognition, filling the gap between findings in human fMRI, non-human primate, and human electrophysiological studies.

Methods

Participants

Forty-seven healthy, right-handed participants were recruited from the local community and the

online participant database (SONA) at the University of Cambridge. Four participants were excluded from the formal analysis due to having behavioural accuracy below 3 standard deviations from the mean. Hence 43 participants (age 18-39 years, 31 females and 12 males) entered the final analysis. All participants were native Mandarin speakers with normal or corrected to normal vision without history of neurological disorders. They gave written informed consent to participate in the study and were paid for their time. The experiment was approved by the Cambridge Psychology Research Ethics Committee. We recruited native Mandarin speakers because we tried to overcome the word-length effects [83] in the WM tasks to balance the difficulty between alphanumeric and colour WM tasks (e.g., "A" or "E" has shorter phonetic length than "red" or "blue" in English while they have the same length in Mandarin, which makes the alphanumeric WM task easier than the colour WM task for English speakers but this difference is less pronounced for Mandarin speakers [84, 85]).

Task design and procedure

To examine potential domain-general activity related to cognitive demand across multiple tasks, we selected three cognitive tasks (WM, SWIT, and MSIT). We manipulated each to have different levels of cognitive demand (hard vs. easy) and different stimuli contents (alphanumeric vs. colour) (Figure 1). As stimuli contents were blocked, we had six subtasks in total (3 tasks * 2 contents).

For the WM task, we used a modified Sternberg task [86]. After a fixation cross was shown for 1.5 +/- 0.1 s, four items (letters for the alphanumeric subtask and coloured circles for the colour subtask) were presented in a horizontal line at the centre of the screen for 0.3 s. In the hard condition the memory set consisted of four unique items, while the set in the easy condition consisted of two unique items flanked by a # (alphanumeric subtask) or black circles (colour subtask). Thus, the physical size and the visual content were the similar in both conditions. After a 2 s delay period, a probe appeared at the centre of the screen and the participant were required to press a button within 2 s to indicate whether the probe was a member of the memory set. We selected the letters from the list "B", "D", "G", "K", "P", "Q", and "R", and selected the colours from red, orange, yellow, green, blue, purple, and pink.

For the SWIT task, after a fixation cross was shown for 1.5 +/- 0.1 s, one item (a two-digit number for the alphanumeric subtask and a coloured circle or triangle in the colour subtask) was presented at the centre of the screen within a square or a diamond for 3 s. For the alphanumeric subtask, if the stimulus was surrounded by a square, participants were instructed to indicate whether it was odd or

even. If the stimulus was surrounded by a diamond, participants were required to indicate whether it could be divided by 3. For the colour subtask, participants were required to indicate whether it was blue or red if the stimulus was surrounded by a square, and to indicate whether it was a circle or a triangle if the stimulus was surrounded by a diamond. Switch trials (the rule for the present trial was different from the last trial) were considered as the hard condition and repeat trials (the rule for the present trial repeated the last trial) were considered as the easy condition. The stimuli were selected from 12, 13, 15, and 16 for the alphanumeric subtask and selected from blue circle, red circle, blue triangle, and red triangle for the colour subtask.

The MSIT task was used as an inhibitory control task. After a fixation cross was shown for 1.5 +/- 0.1 s, a row of three items (digits for the alphanumeric subtask and coloured circles for the colour subtask) were presented at the centre of the screen for 3 s. Participants were required to identify the unique item among the three items and to press a button with one of three fingers as quickly as possible and within 3 s. The target item was “1”, “2”, or “3” for the alphanumeric subtask and was “red”, “green”, and “blue” for the colour subtask. Participants underwent a practice to match “1”, “2”, and “3” (or “red”, “green”, and “blue”) to three buttons. In the hard (incongruent) condition, the target item was presented in the position incongruent with the original value (e.g., “1” or “red” presented at the third position), and always flanked by different interfering numbers or colours (e.g., “331” or “blue, blue, red”). In the easy (congruent) condition, the target item was presented in the position compatible with its original value and flanked by 0 or “X” in the alphanumeric subtask (e.g., “100” or “1XX”) while flanked by black circles in the colour subtask (e.g., “red, black, black”).

Participants performed two runs of each subtask, yielding a total of 12 runs for each participant. Each run included two blocks of the same subtask, with 36 trials per block for the WM and MSIT tasks. For the SWIT task, each block included 37 trials, but the first trial of each block was dropped, resulting in 36 trials per block for analysis. For all tasks, trials in each block were randomized and equally split between easy and hard trials. For the WM task, there were equal numbers of positive (probe on the list) and negative trials (probe not on the list) and these trials were randomly intermixed. Participants were allowed to take short breaks between blocks and between runs. The sequence of the three tasks (WM, SWIT, and MSIT) was counterbalanced across participants to control for order effects. Within each task, participants completed a run of each type of subtask once before repeating it. The order of subtask presentation was counterbalanced across participants.

MEG/EEG data acquisition and preprocessing

We used concurrent MEG and EEG to maximize spatial resolution for later source estimation [87, 88]. MEG data were acquired in a magnetically shielded room with a Neuromag Vectorview system (Elekta AB, Stockholm, Sweden) with 306 channels (204 planar gradiometers and 102 magnetometers). EEG data were acquired concurrently using a 70-channel MEG-compatible EEG cap (EasyCap GmbH, Herrsching, Germany) with an extended 10-10 electrode layout. EEG reference and ground electrodes were attached to the left side of the nose and the left cheek, respectively. We recorded electrooculogram (EOG) by placing electrodes above and below the right eye (vertical EOG) and at the outer canthi (horizontal EOG). We also recorded electrocardiogram (ECG) by placing electrodes to the bottom left of ribcage and the right clavicle. For the co-registration with MRI structural data, we used a 3D digitizer (3SpaceIsotrakIISystem, Polhemus, Colchester, Vermont, USA) to record the positions of 5 head position indicator (HPI) coils, EEG electrodes, and 80-200 additional points covering the whole EEG cap, relative to three anatomic fiducial points (nasion and left and right preauricular points). Data were acquired with a sampling rate of 1000 Hz with a band-pass filter of 0.03-330 Hz.

We used MNE-Python [89] for all the processing steps. First, we applied the Signal-Space Separation (SSS) to the raw MEG data to reduce environmental artefacts [90]. This step also involved head movement compensation and bad channel repair for MEG data. Then, we visually inspected the raw data for each participant and marked bad EEG channels, which were excluded from further analysis. To reduce the eye movement and cardiac artefacts, we performed an independent component analysis (ICA) using the FastICA algorithm [91] for each participant after concatenating data from all the runs. Before running the ICA, the data was downsampled to 200 Hz and filtered between 1 and 40 Hz to improve ICA performance [92]. The first n components explaining the cumulative variance of 95% of the data were entered into the ICA. We applied the computed ICA filters to the raw data (not down-sampled or filtered) and removed eye movement and heart-beat artefacts from both MEG and EEG. We identified EOG- and ECG-related components using correlations between components and the EOG/ECG channel, with components above the threshold (z-scores > 3) masked as EOG- or ECG-related and removed. After ICA, we filtered the data to 1-40 Hz, re-referenced the EEG data to the channel average, and divided data into epochs from -1 to 2 seconds from stimulus onset. We rejected epochs with excessive noise if their peak-to-peak amplitudes were higher than the following thresholds: 350 μV for EEG, 5000 fT for magnetometers, and 4000 fT/cm for gradiometers. Incorrect or overtime

trials were also rejected. Using this procedure a total of 67 out of 868 trials (7.72%) on average were excluded from further analysis.

Source reconstruction

For each participant, a T1-weighted MRI structural scan was acquired using a Siemens 3T Prisma scanner. We used the automated segmentation algorithms in FreeSurfer (http://surfer.nmr.mgh.harvard.edu/) to obtain the reconstructed scalp surface [93]. Then, we used MNE-Python to compute forward and inverse models. We used a three-layer boundary element model (BEM) to compute the forward model of each participant's scalp, outer skull surface, and inner skull surface using default conductivity parameters (0.3, 0.006, and 0.3, respectively). The MEG/EEG sensor configurations and MRI structural images were co-registered by matching the scalp digitization points to the scalp surface. For source analyses on task demand, we calculated noise covariance matrices for each participant and each task based on the pre-stimulus baseline period (-400 to -100 ms from the stimulus onset). For source analyses on task content, we calculated noise covariance matrices based on a 10-second period from the empty room data recorded on the testing day. This is because the task contents were blocked meaning the pre-stimulus time periods was not an ideal baseline in this case. Then, we selected the best estimator of the noise covariance matrices among a list of methods ("shrunk", "empirical", "factor_analysis", and "diagonal_fixed") based on the log-likelihood and cross-validation separately for each participant and analysis (demand/content), using the automatic method embedded in *mne.compute_covariance* function [94]. The inverse operator was obtained for each participant and each task using dynamic statistical parametric mapping [95] (dSPM) with a loose orientation constraint value of 0.2 and without depth weighting. We used the default SNR = 3.0 to regularize the inverse operator. In order to perform group analyses, we morphed individual source space data to the standard average brain (fsaverage), yielding time courses of activity for 10242 vertices in each hemisphere for each participant. We parcellated the standard fsaverage brain to 360 regions (180 regions per hemisphere without the medial wall) based on the Human Connectome Project multimodal parcellation (HCP-MMP1.0) [53] by averaging values of each vertex within each parcel using the *'mean_flip'* mode. The *'mean_flip'* mode finds the dominant direction of source space normal vector orientations for each parcel and applies a sign-flip to vertices whose orientation is more than 90° different from the dominant direction, and then averages across vertices within each parcel.

Multivariate pattern analysis (MVPA)

For MVPA in sensor space, we used the data from all the MEG and EEG sensors (306 MEG sensors and 64 EEG channels). We used MNE-Python[89] and the Scikit-learn package[96] in Python for the analysis. To reduce computation time, we downsampled the data to 200 Hz. After removing the evoked potentials (i.e., the average signal across trials) from each trial for each condition[29], we used IRASA [50] to separate the oscillatory and the aperiodic components from the mixed power spectrum using the time window of 0.3-1.5 s relative to stimulus onset for each subtask. We used a recommended set of resampling factors (*h*) from 1.1 to 1.9 with the linear space of 0.05 [50]. With the 200 Hz sampling rate and the maximum resampling factors we chose, frequencies up to 50 Hz were able to be estimated. Thus, we estimated the frequencies from 1 to 30 Hz with 1 Hz steps covering all the frequency bands of interest. After obtaining the aperiodic spectrum from IRASA, we subtracted it from the mixed spectrum to obtain the oscillatory spectrum. To obtain the oscillatory power for further analyses, we averaged the power for each frequency band using the ranges theta: 3-7 Hz; alpha: 8-12 Hz; and beta: 15-30 Hz. For aperiodic broadband power, we averaged the aperiodic spectrum power across 3-30 Hz. To obtain the slope and intercept of the aperiodic components, we used the least squares estimation to fit a linear function to the estimated aperiodic power spectrum in log-log coordinates, extracting the slope and the intercept for later analyses.

To increase the signal-to-noise rate of MVPA, we averaged every 4 trials into "pseudo-trials" for each condition (e.g., hard or easy condition in the colour WM subtask) using a random selection of the available trials [97]. When the number of trials was not divisible by 4, we excluded the remainder trials. If the number of resulting pseudo-trials was not the same for the two conditions, we equated them by removing pseudo-trials from the condition with more. Then, the data for each channel were standardized by subtracting the mean and dividing by the standard deviation across epochs. We then used a 5-fold cross-validation procedure for MVPA classification with a linear support vector machine (SVM) for each frequency band or aperiodic component, where the pseudo-trials were randomly divided into 5 parts, of which 4 were used for training and 1 for testing. The cross-validation procedure was repeated 5 times such that all pseudo-trials were used equally for training and testing. After splitting the data into folds, we performed PCA across sensors to retain components accounting for 99% of the variance and used those principal components for classification. Specifically, for each iteration, we performed PCA on the training fold (i.e., 4 folds altogether) and then transformed the

testing fold using the same PCA components. The decoding results (the area under the receiver-operating curve; AUC) across those 5 iterations were averaged together. To ensure the results were not dependent on a specific set of trial averages, we repeated the entire procedure 25 times per participant and averaged the AUC over these repetitions to give the final AUC for statistical testing. The MVPA procedure was performed on each subtask based on either oscillatory components or aperiodic components separately. We classified hard vs. easy trials for each subtask for demand decoding and classified alphanumeric vs. colour trials for each task for content decoding.

To estimate the source patterns underpinning each classification, we used the weight projection method [54]. We first repeated the same decoding analysis, now based on the 360 ROIs in source space, using the same procedure described above. Classification weights for each ROI indicated how much the information measured in that region was used by a classifier to separate the classes (e.g., hard vs. easy). To interpret these weights in a meaningful way, we transformed them to the activation patterns by multiplying the weights by the covariance of the data [54]. The transformed weights are equivalent to the univariate response in each contrast (e.g., hard vs. easy) and are informative to identify brain regions that contributed to the most to the classification. Positive patterns indicate increased activity in the hard condition (or the colour condition for content decoding) compared to the easy condition (or the alphanumeric condition for content decoding), and vice versa [54]. For averaged results across subtasks, we z-scored the data across all ROIs and then averaged the z-scored data across participants and subtasks.

Cross-task generalisation

For the cross-task generalisation in the sensor space, we trained MVPA classifiers based on one subtask using all MEG/EEG sensors and then tested them in all other subtasks, yielding a training subtask * testing subtask matrix. We used the same decoding settings (e.g., pseudo-trials) as described above, except that here we used all the data from each subtask without splitting them into 5 folds. This procedure was done for each aperiodic and oscillatory signal separately. The off-diagonal results showed the average of the generalisation performance between two specific train-test schemes within a pair of subtasks (e.g., training on alphanumeric WM task, testing on colour SWIT task, and training on colour SWIT task, testing on alphanumeric WM task), with significantly above-chance AUC meaning the signal was generalisable across the two tasks.

Representation geometry in the state space

Representation geometry analysis was done in sensor space. To visualize how the signals simultaneously represented task demand and content information, we first averaged trials within each condition (12 conditions in total: 3 tasks * 2 demands * 2 contents) for each sensor and each signal, then did PCA to extract the first two PCs for each condition and signal. To average results across tasks, we aligned each participant's PCs of different tasks using Procrustes transformation (without a scaling component) and then averaged aligned PCs across tasks. Then, Procrustes transformation without a scaling component was again used to align the PCs of different participants for visualizing the averaged results across participants.

Statistical analysis

All statistical analyses were performed in Python. We used repeated measures ANOVAs for the behavioural analysis, used Pearson's correlation for the correlation analysis, and used one-sample *t* tests for all other tests. The Benjamini-Hochberg (BH) procedure was used to control the false discovery rate (FDR) for the *t* tests for each analysis in the results, and we reported the significant results with corrected $p < 0.05$ for these tests. To test the significance of the mean correlation coefficient across participants, we conducted permutation tests with 1000 iterations. For each permutation, the labels of one variable were randomly shuffled within each participant's data. Pearson's correlation coefficients were computed for both the original and permuted data sets. We averaged correlation coefficients over participants per permutation, yielding a null distribution of permutated mean correlation coefficients across participants after 1000 permutations. The significance of the observed mean correlation was determined by comparing it to the null distribution generated from the permutations. One-tailed tests were used for the decoding analysis classifying task demand or content, since below-chance decoding is uninterpretable. Otherwise, two-tailed tests were used.

Acknowledgements

This project was supported by UKRI MRC intramural funding (SUAG/093/G116768) to A.W., and a Gates Cambridge Scholarship awarded to R.L. (OPP1144). The authors thank Olaf Hauk and Máté Aller for their suggestions on MEG/EEG data processing. For the purpose of open access, the author has applied a Creative Commons Attribution (CC BY) licence to any Author Accepted Manuscript version arising from this submission.

Author Contributions

R.L., and A.W. conceived the project; R.L., J.D., and A.W. designed the experiment; R.L., N.D., and A.W. implemented the experiment; R.L. conducted the experiment; R.L., N.D., and A.W. analysed data; R.L. wrote the first draft of the paper; R.L., N.D., J.D., and A.W. contributed to the final draft of the paper; A.W. provided overall supervision; and A.W. and R.L contributed funding.

Declaration of interests

The authors declare no competing interests.

Supplementary

Table S1 Descriptive statistics: Mean and standard deviation (in brackets) of response error and response time (RT), N = 43

		WM		SWIT		MSIT	
		Easy	Hard	Easy	Hard	Easy	Hard
Accuracy (%)	Alphanumeric	96.48 (4.99)	91.15 (8.63)	96.81 (2.94)	95.74 (3.38)	99.84 (0.54)	96.71 (3.46)
	Colour	96.22 (4.65)	84.98 (6.45)	96.82 (2.86)	95.65 (4.01)	99.64 (0.81)	97.38 (2.29)
RT (ms)	Alphanumeric	652 (111)	769 (135)	1032 (169)	1173 (200)	581 (103)	799 (148)
	Colour	603 (113)	732 (139)	1007 (172)	1170 (205)	615 (123)	828 (158)

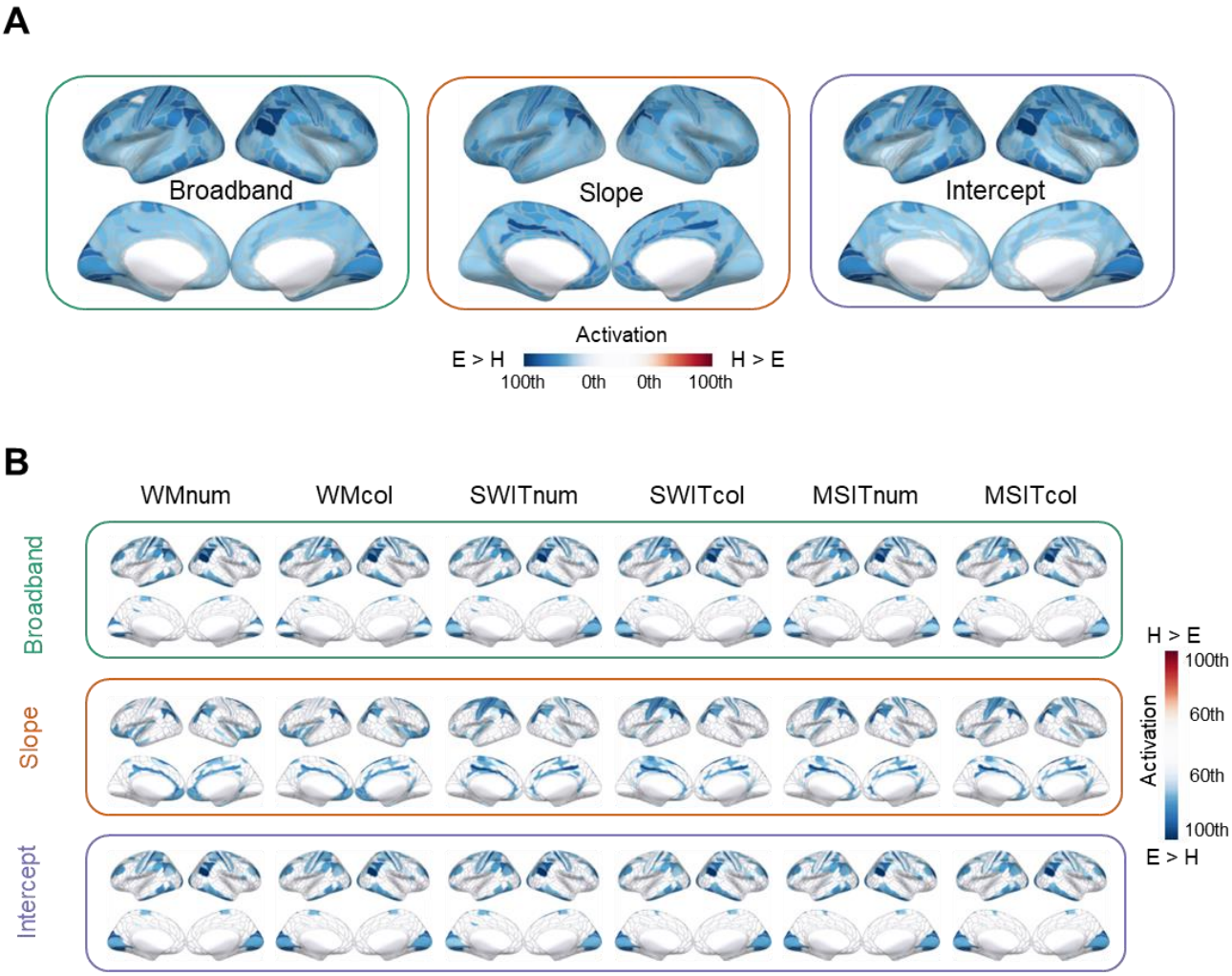

Figure S1. (A) The full map of source estimation patterns for demand decoding (hard vs. easy) averaged across all the subtasks for aperiodic signals. Outlines show 360 cortical regions based on the Human Connectome Project multimodal parcellation (HCP-MMP1.0) [53]. Coloured regions represent the 0th to 100th percentiles of activation across the brain (H: hard; E: easy). (B) Source estimation patterns for demand decoding (hard vs. easy) in each subtask for the aperiodic components. Coloured regions represent the 60th to 100th percentiles of activation across the brain. Abbreviations as shown in Figure 2.

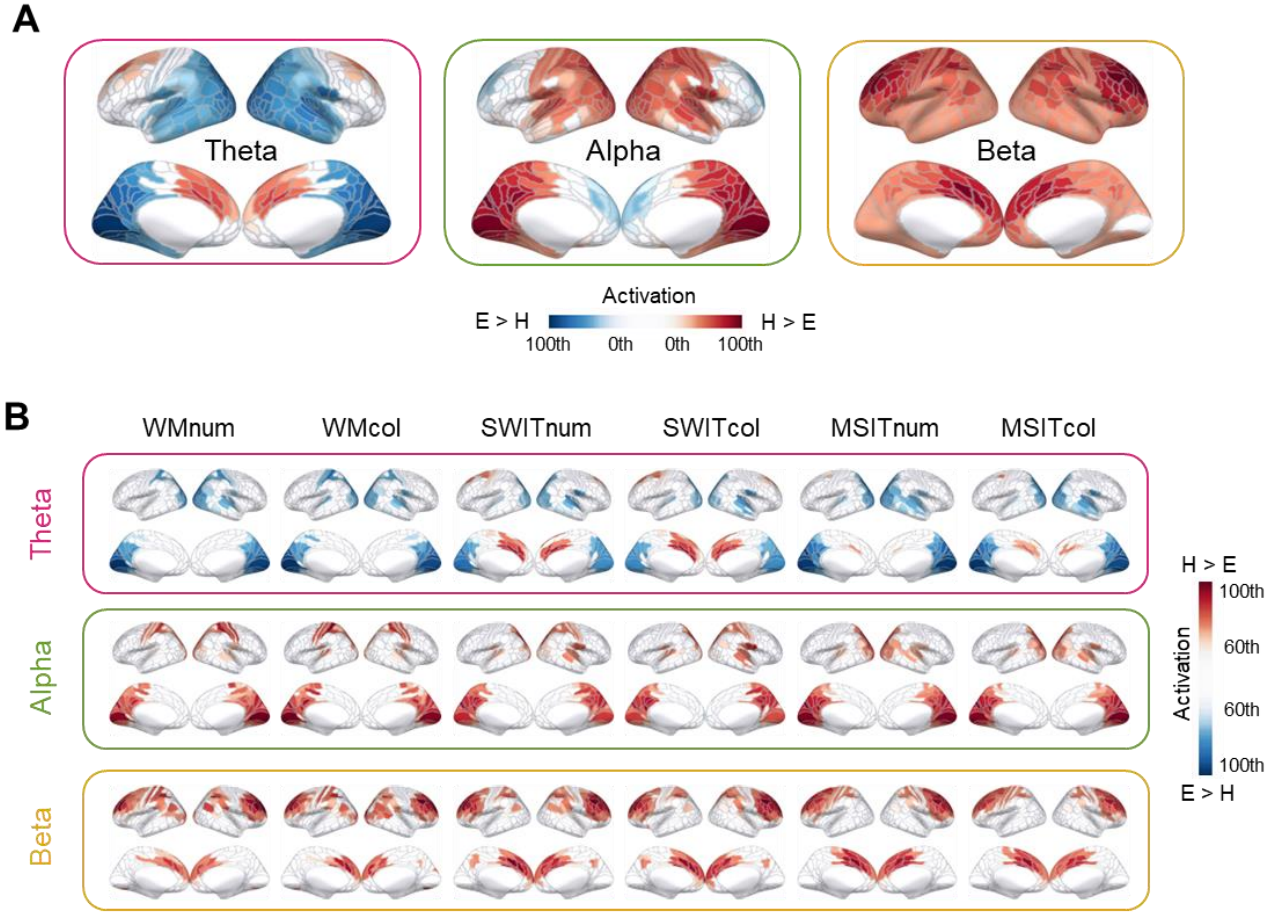

Figure S2. (A) The full map of source estimation patterns for demand decoding (hard vs. easy) averaged across all the subtasks for oscillatory signals. Coloured regions represent the 0th to 100th percentiles of activation across the brain (H: hard; E: easy). (B) Source estimation patterns for demand decoding (hard vs. easy) in each subtask for the oscillatory components. Coloured regions represent the 60th to 100th percentiles of activation across the brain. Abbreviations as shown in Figure 2.

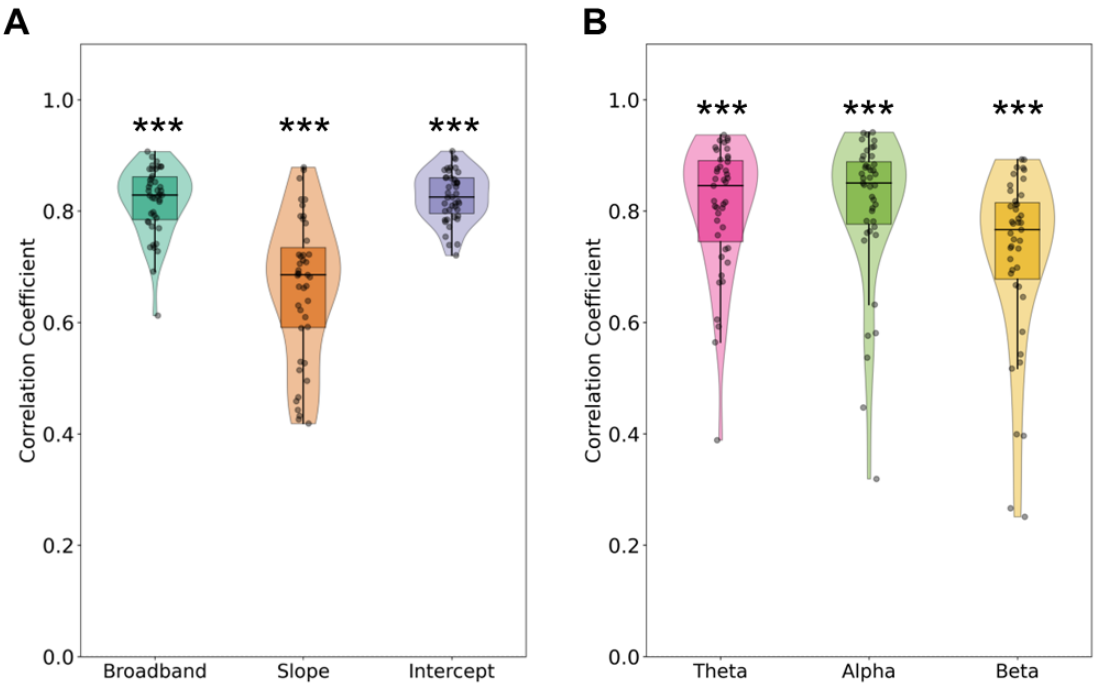

Figure S3. Pearson's correlation results between source estimation patterns that coded demand and content from (A) aperiodic and (B) oscillatory activity across 360 cortical regions in source space. All the signals were averaged across subtasks per region before calculating the correlations. Each dot represents a single participant. *** $p < 0.001$ with 1000 permutations.

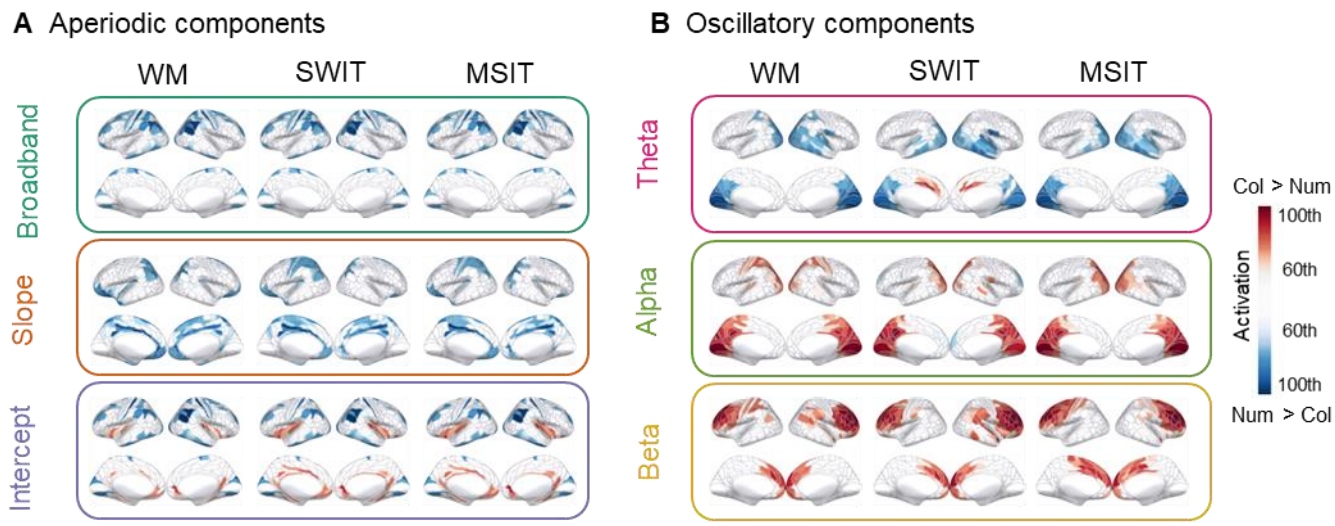

Figure S4. Source estimation patterns for task content decoding (alphanumeric vs. colour) for each task based on (A) the aperiodic and (B) the oscillatory activity. Coloured regions represent the 60th to 100th percentiles of activation across the brain. Abbreviations as shown in Figure 2.

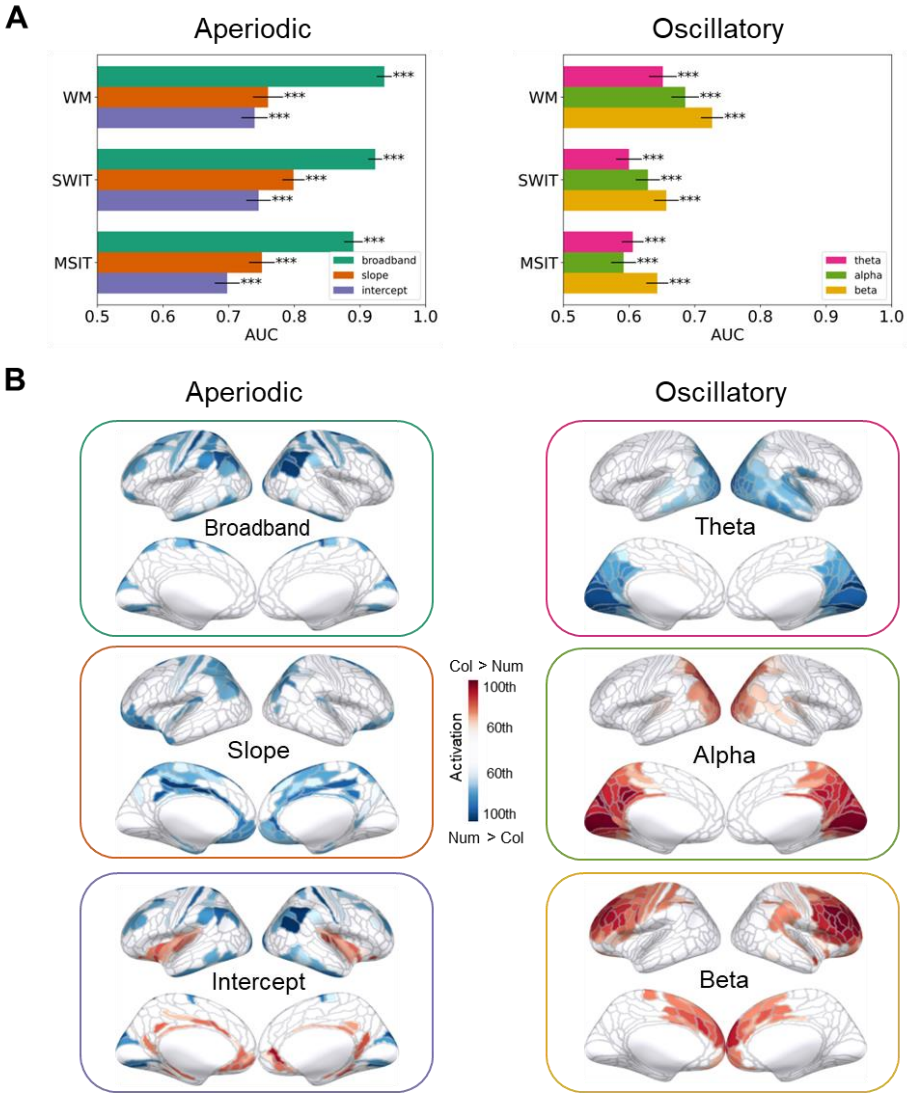

Figure S5. (A) Decoding results on task content (alphanumeric vs. colour) using easy trials only based on the aperiodic and oscillatory activity. (B) Source estimation patterns averaged across all the tasks using easy trials only based on the aperiodic and oscillatory activity. Coloured regions represent the 60th to 100th percentiles of activation across the brain. Abbreviations as shown in Figure 2.

References

1. Duncan, J., M. Assem, and S. Shashidhara, *Integrated Intelligence from Distributed Brain Activity.* Trends Cogn Sci, 2020. **24**(10): p. 838-852.
2. Fedorenko, E., J. Duncan, and N. Kanwisher, *Broad domain generality in focal regions of frontal and parietal cortex.* Proc Natl Acad Sci U S A, 2013. **110**(41): p. 16616-21.
3. Kanwisher, N., *The Quest for the FFA and Where It Led.* J Neurosci, 2017. **37**(5): p. 1056-61.
4. Cole, M.W. and W. Schneider, *The cognitive control network: Integrated cortical regions with dissociable functions.* Neuroimage, 2007. **37**(1): p. 343-60.
5. Dosenbach, N.U., et al., *A core system for the implementation of task sets.* Neuron, 2006. **50**(5): p. 799-812.
6. Duncan, J. and A.M. Owen, *Common regions of the human frontal lobe recruited by diverse cognitive demands.* Trends in neurosciences, 2000. **23**(10): p. 475-483.
7. Gratton, C., H. Sun, and S.E. Petersen, *Control networks and hubs.* Psychophysiology, 2018. **55**(3).
8. Assem, M., et al., *A Domain-General Cognitive Core Defined in Multimodally Parcellated Human Cortex.* Cereb Cortex, 2020. **30**(8): p. 4361-4380.
9. Duncan, J., *The multiple-demand (MD) system of the primate brain: mental programs for intelligent behaviour.* Trends in Cognitive Sciences, 2010. **14**(4): p. 172-179.
10. Donoghue, T., et al., *Parameterizing neural power spectra into periodic and aperiodic components.* Nat Neurosci, 2020. **23**(12): p. 1655-1665.
11. He, B.J., *Scale-free brain activity: past, present, and future.* Trends Cogn Sci, 2014. **18**(9): p. 480-7.
12. Donoghue, T., N. Schaworonkow, and B. Voytek, *Methodological considerations for studying neural oscillations.* Eur J Neurosci, 2022. **55**(11-12): p. 3502-3527.
13. Gao, R., E.J. Peterson, and B. Voytek, *Inferring synaptic excitation/inhibition balance from field potentials.* Neuroimage, 2017. **158**: p. 70-78.
14. Waschke, L., et al., *Modality-specific tracking of attention and sensory statistics in the human electrophysiological spectral exponent.* eLife, 2021. **10**: p. e70068.
15. Wen, H. and Z. Liu, *Broadband Electrophysiological Dynamics Contribute to Global Resting-State fMRI Signal.* J Neurosci, 2016. **36**(22): p. 6030-40.
16. Jacob, M.S., et al., *Aperiodic measures of neural excitability are associated with anticorrelated hemodynamic networks at rest: A combined EEG-fMRI study.* Neuroimage, 2021. **245**: p. 118705.
17. Gyurkovics, M., et al., *Stimulus-induced changes in 1/f-like background activity in EEG.* J Neurosci, 2022. **42**(37): p. 7144-51.
18. Thuwal, K., A. Banerjee, and D. Roy, *Aperiodic and Periodic Components of Ongoing Oscillatory Brain Dynamics Link Distinct Functional Aspects of Cognition across Adult Lifespan.* eNeuro, 2021. **8**(5).
19. Ouyang, G., et al., *Decomposing alpha and 1/f brain activities reveals their differential associations with cognitive processing speed.* Neuroimage, 2020. **205**: p. 116304.
20. Podvalny, E., et al., *A unifying principle underlying the extracellular field potential spectral responses in the human cortex.* J Neurophysiol, 2015. **114**(1): p. 505-19.
21. Helfrich, R.F., J.D. Lendner, and R.T. Knight, *Aperiodic sleep networks promote memory consolidation.* Trends Cogn Sci, 2021. **25**(8): p. 648-659.
22. Pei, L., G. Northoff, and G. Ouyang, *Comparative analysis of multifaceted neural effects associated with varying endogenous cognitive load.* Commun Biol, 2023. **6**(1): p. 795.
23. Cavanagh, J.F. and M.J. Frank, *Frontal theta as a mechanism for cognitive control.* Trends Cogn Sci, 2014. **18**(8): p. 414-21.

24. Chikhi, S., N. Matton, and S. Blanchet, *EEG power spectral measures of cognitive workload: A meta-analysis.* Psychophysiology, 2022. **59**(6): p. e14009.
25. Pavlov, Y.G. and B. Kotchoubey, *Oscillatory brain activity and maintenance of verbal and visual working memory: A systematic review.* Psychophysiology, 2022. **59**(5): p. e13735.
26. Roux, F. and P.J. Uhlhaas, *Working memory and neural oscillations: alpha-gamma versus theta-gamma codes for distinct WM information?* Trends Cogn Sci, 2014. **18**(1): p. 16-25.
27. Cooper, P.S., et al., *Frontal theta predicts specific cognitive control-induced behavioural changes beyond general reaction time slowing.* Neuroimage, 2019. **189**: p. 130-140.
28. Cooper, P.S., et al., *Frontoparietal theta oscillations during proactive control are associated with goal-updating and reduced behavioral variability.* Biol Psychol, 2017. **129**: p. 253-264.
29. Cohen, M.X. and T.H. Donner, *Midfrontal conflict-related theta-band power reflects neural oscillations that predict behavior.* J Neurophysiol, 2013. **110**(12): p. 2752-63.
30. Eisma, J., et al., *Frontal midline theta differentiates separate cognitive control strategies while still generalizing the need for cognitive control.* Sci Rep, 2021. **11**(1): p. 14641.
31. Nigbur, R., G. Ivanova, and B. Sturmer, *Theta power as a marker for cognitive interference.* Clin Neurophysiol, 2011. **122**(11): p. 2185-94.
32. Muckschel, M., G. Dippel, and C. Beste, *Distinguishing stimulus and response codes in theta oscillations in prefrontal areas during inhibitory control of automated responses.* Hum Brain Mapp, 2017. **38**(11): p. 5681-5690.
33. Brouwer, A.M., et al., *Evidence for effects of task difficulty but not learning on neurophysiological variables associated with effort.* Int J Psychophysiol, 2014. **93**(2): p. 242-52.
34. Fukuda, K., I. Mance, and E.K. Vogel, *alpha Power Modulation and Event-Related Slow Wave Provide Dissociable Correlates of Visual Working Memory.* J Neurosci, 2015. **35**(41): p. 14009-16.
35. Gevins, A., et al., *High-resolution EEG Mapping of Cortical Activation Related to Working Memory: Effects of Task Difficulty, Type of Processing, and Practice.* Cereb Cortex, 1997. **7**(4): p. 374-385.
36. Cooper, P.S., et al., *Contextually sensitive power changes across multiple frequency bands underpin cognitive control.* Neuroimage, 2016. **132**: p. 499-511.
37. Proskovec, A.L., A.I. Wiesman, and T.W. Wilson, *The strength of alpha and gamma oscillations predicts behavioral switch costs.* Neuroimage, 2019. **188**: p. 274-281.
38. Sauseng, P., et al., *Relevance of EEG alpha and theta oscillations during task switching.* Exp Brain Res, 2006. **170**(3): p. 295-301.
39. Bastos, A.M., et al., *Visual areas exert feedforward and feedback influences through distinct frequency channels.* Neuron, 2015. **85**(2): p. 390-401.
40. Lundqvist, M., et al., *Gamma and beta bursts during working memory readout suggest roles in its volitional control.* Nat Commun, 2018. **9**(1): p. 394.
41. Schmidt, R., et al., *Beta Oscillations in Working Memory, Executive Control of Movement and Thought, and Sensorimotor Function.* J Neurosci, 2019. **39**(42): p. 8231-8238.
42. Stoll, F.M., et al., *The Effects of Cognitive Control and Time on Frontal Beta Oscillations.* Cereb Cortex, 2016. **26**(4): p. 1715-1732.
43. Duncan, J., *An adaptive coding model of neural function in prefrontal cortex.* Nature reviews neuroscience, 2001. **2**(11): p. 820-829.
44. Zheng, Y., R. Lu, and A. Woolgar, *Radical flexibility of neural representation in frontoparietal cortex and the challenge of linking it to behaviour.* Current Opinion in Behavioral Sciences, 2024. **57**: p. 101392.
45. Woolgar, A., J. Jackson, and J. Duncan, *Coding of Visual, Auditory, Rule, and Response Information in the Brain: 10 Years of Multivoxel Pattern Analysis.* J Cogn Neurosci, 2016. **28**(10): p. 1433-54.

46. Woolgar, A., et al., *Multi-voxel coding of stimuli, rules, and responses in human frontoparietal cortex.* Neuroimage, 2011. **56**(2): p. 744-52.
47. Badre, D., et al., *The dimensionality of neural representations for control.* Curr Opin Behav Sci, 2021. **38**: p. 20-28.
48. Rigotti, M., et al., *The importance of mixed selectivity in complex cognitive tasks.* Nature, 2013. **497**(7451): p. 585-90.
49. Fusi, S., E.K. Miller, and M. Rigotti, *Why neurons mix: high dimensionality for higher cognition.* Curr Opin Neurobiol, 2016. **37**: p. 66-74.
50. Wen, H. and Z. Liu, *Separating Fractal and Oscillatory Components in the Power Spectrum of Neurophysiological Signal.* Brain Topogr, 2016. **29**(1): p. 13-26.
51. Grootswagers, T., S.G. Wardle, and T.A. Carlson, *Decoding Dynamic Brain Patterns from Evoked Responses: A Tutorial on Multivariate Pattern Analysis Applied to Time Series Neuroimaging Data.* J Cogn Neurosci, 2017. **29**(4): p. 677-697.
52. Peelen, M.V. and P.E. Downing, *Testing cognitive theories with multivariate pattern analysis of neuroimaging data.* Nat Hum Behav, 2023. **7**(9): p. 1430-1441.
53. Glasser, M.F., et al., *A multi-modal parcellation of human cerebral cortex.* Nature, 2016. **536**(7615): p. 171-178.
54. Haufe, S., et al., *On the interpretation of weight vectors of linear models in multivariate neuroimaging.* Neuroimage, 2014. **87**: p. 96-110.
55. Duncan, J., *The structure of cognition: attentional episodes in mind and brain.* Neuron, 2013. **80**(1): p. 35-50.
56. Bassett, D.S., et al., *Adaptive reconfiguration of fractal small-world human brain functional networks.* Proceedings of the National Academy of Sciences, 2006. **103**(51): p. 19518-19523.
57. He, B.J., et al., *The temporal structures and functional significance of scale-free brain activity.* Neuron, 2010. **66**(3): p. 353-69.
58. Molina, J.L., et al., *Memantine Effects on Electroencephalographic Measures of Putative Excitatory/Inhibitory Balance in Schizophrenia.* Biol Psychiatry Cogn Neurosci Neuroimaging, 2020. **5**(6): p. 562-568.
59. Robertson, M.M., et al., *EEG power spectral slope differs by ADHD status and stimulant medication exposure in early childhood.* J Neurophysiol, 2019. **122**(6): p. 2427-2437.
60. Voytek, B., et al., *Oscillatory dynamics coordinating human frontal networks in support of goal maintenance.* Nat Neurosci, 2015. **18**(9): p. 1318-24.
61. Frelih, T., et al., *Modulation of aperiodic EEG activity provides sensitive index of cognitive state changes during working memory task.* BioRXiv, 2024.
62. Kardan, O., et al., *Distinguishing cognitive effort and working memory load using scale-invariance and alpha suppression in EEG.* Neuroimage, 2020. **211**: p. 116622.
63. Churchill, N.W., et al., *The suppression of scale-free fMRI brain dynamics across three different sources of effort: aging, task novelty and task difficulty.* Sci Rep, 2016. **6**: p. 30895.
64. Clayton, M.S., N. Yeung, and R. Cohen Kadosh, *The many characters of visual alpha oscillations.* Eur J Neurosci, 2018. **48**(7): p. 2498-2508.
65. Keitel, C., et al., *Rhythms in cognition: The evidence revisited.* Eur J Neurosci, 2022. **55**(11-12): p. 2991-3009.
66. Keil, A., et al., *Recommendations and publication guidelines for studies using frequency domain and time-frequency domain analyses of neural time series.* Psychophysiology, 2022. **59**(5): p. e14052.
67. Brookes, M.J., et al., *Changes in brain network activity during working memory tasks: a magnetoencephalography study.* Neuroimage, 2011. **55**(4): p. 1804-15.
68. Jensen, O. and C.D. Tesche, *Frontal theta activity in humans increases with memory load in a working memory.* European Journal of Neuroscience, 2002. **15**: p. 1395-99.

69. Lu, R., et al., *High fluid intelligence is characterized by flexible allocation of attentional resources: Evidence from EEG.* Neuropsychologia, 2022. **164**: p. 108094.
70. Meltzer, J.A., et al., *Individual differences in EEG theta and alpha dynamics during working memory correlate with fMRI responses across subjects.* Clin Neurophysiol, 2007. **118**(11): p. 2419-36.
71. Misselhorn, J., U. Friese, and A.K. Engel, *Frontal and parietal alpha oscillations reflect attentional modulation of cross-modal matching.* Sci Rep, 2019. **9**(1): p. 5030.
72. Jensen, O., et al., *Oscillations in the Alpha Band (9–12 Hz) Increase with Memory Load during Retention in a Short-term Memory Task.* Cerebral Cortex, 2002. **12**(8): p. 877-882.
73. Jensen, O., *Gating by alpha band inhibition revised: a case for a secondary control mechanism.* PsyArXiv, 2023.
74. Scheeringa, R., et al., *Trial-by-trial coupling between EEG and BOLD identifies networks related to alpha and theta EEG power increases during working memory maintenance.* Neuroimage, 2009. **44**(3): p. 1224-38.
75. Jensen, O. and A. Mazaheri, *Shaping functional architecture by oscillatory alpha activity: gating by inhibition.* Front Hum Neurosci, 2010. **4**: p. 186.
76. Buschman, T.J. and E.K. Miller, *Top-down versus bottom-up control of attention in the prefrontal and posterior parietal cortices.* Science, 2007. **315**(5820): p. 1860-2.
77. Siegel, M., T.H. Donner, and A.K. Engel, *Spectral fingerprints of large-scale neuronal interactions.* Nat Rev Neurosci, 2012. **13**(2): p. 121-34.
78. Ebitz, R.B. and B.Y. Hayden, *The population doctrine in cognitive neuroscience.* Neuron, 2021. **109**(19): p. 3055-3068.
79. Weber, J., et al., *Subspace partitioning in the human prefrontal cortex resolves cognitive interference.* Proc Natl Acad Sci U S A, 2023. **120**(28): p. e2220523120.
80. Klimesch, W., *EEG alpha and theta oscillations reflect cognitive and memory performance: a review and analysis.* Brain Research Reviews, 1999. **29**: p. 169-195.
81. Riddle, J., et al., *Causal Evidence for a Role of Theta and Alpha Oscillations in the Control of Working Memory.* Curr Biol, 2020. **30**(9): p. 1748-1754 e4.
82. Wendiggensen, P., et al., *Interplay between alpha and theta band activity enables management of perception-action representations for goal-directed behavior.* Commun Biol, 2023. **6**(1): p. 494.
83. Baddeley, A., N. Thomson, and M. Buchanan, *Word length and the structure of short-term memory.* Journal of Verbal Learning and Verbal Behavior, 1975. **4**(6): p. 575-589.
84. Chan, M.E. and J.M. Elliott, *Cross -Linguistic Differences in Digit Memory Span.* Australian Psychologist, 2020. **46**(1): p. 25-30.
85. Stigler, J.W., S.-Y. Lee, and H.W. Stevenson, *Digit memory in Chinese and English: Evidence for a temporally limited store.* Cognition, 1986. **23**(1): p. 1-20.
86. Sternberg, S., *High-Speed Scanning in Human Memory.* Science, 1966. **153**(3736): p. 652-654.
87. Henson, R.N., E. Mouchlianitis, and K.J. Friston, *MEG and EEG data fusion: simultaneous localisation of face-evoked responses.* Neuroimage, 2009. **47**(2): p. 581-9.
88. Hauk, O., M. Stenroos, and M.S. Treder, *Towards an objective evaluation of EEG/MEG source estimation methods - The linear approach.* Neuroimage, 2022. **255**: p. 119177.
89. Gramfort, A., et al., *MEG and EEG data analysis with MNE-Python.* Front Neurosci, 2013. **7**: p. 267.
90. Taulu, S. and M. Kajola, *Presentation of electromagnetic multichannel data: The signal space separation method.* Journal of Applied Physics, 2005. **97**(12): p. 124905.
91. Hyvärinen, A. and E. Oja, *Independent component analysis: algorithms and applications.* Neural Networks, 2000. **13**(4-5): p. 411-430.
92. Winkler, I., et al., *On the influence of high-pass filtering on ICA-based artifact reduction in EEG-ERP*, in

Engineering in Medicine and Biology Society (EMBC). 2015, IEEE: Milan. p. 4101–4105.

93. Dale, A.M., B. Fischl, and M.I. Sereno, *Cortical Surface-Based Analysis. I. Segmentation and surface reconstruction.* Neuroimage, 1999. **9**(2): p. 179-194.
94. Engemann, D.A. and A. Gramfort, *Automated model selection in covariance estimation and spatial whitening of MEG and EEG signals.* Neuroimage, 2015. **108**: p. 328-42.
95. Dale, A.M., et al., *Dynamic Statistical Parametric Mapping: Combining fMRI and MEG for High-Resolution Imaging of Cortical Activity.* Neuron, 2000. **26**(1): p. 55-67.
96. Pedregosa, F., et al., *Scikit-learn: Machine Learning in Python.* Journal of Machine Learning Research, 2011. **12**: p. 2825-2830.
97. Scrivener, C.L., T. Grootswagers, and A. Woolgar, *Optimising analysis choices for multivariate decoding: Creating pseudotrials using trial averaging and resampling.* BioRXiv, 2023.